Journal of Visualization, Vol. 3, No. 2 (2000) 175-185

Velocity Measurements in a Turbulent Round Jet Using PTV: the Effect of Tracer Particles

Romano, G. P.* and Zincone, S.*

* Department of Mechanics and Aeronautics, University of Roma "La Sapienza," Roma, Italy.

Received 7 January 2000.
Revised 8 May 2000.

***Abstract*:** The effects of different tracer particles used in the PTV technique on the velocity field are investigated. The measurements are taken in a water round jet at a Reynolds number equal to about 40000, a flow field widely examined in the literature, in which strong velocity differences are encountered. The interest is focused onto particles with different density. Although the mean and rms values are almost unaffected, both measurements obtained with light and heavy particles (in comparison to the density of the fluid) reveal a modified velocity field. The moments of velocity differences (structure functions) point out that such a modification is felt within each range of flow scales. Particles with density almost equal to that of the fluid reproduce the flow behaviour over all the scales.

***Keywords*:** PTV, seeding particles, round jet, velocity differences.

1. Introduction

The PIV (Particle Image Velocimetry) and PTV (Particle Tracking Velocimetry) velocity measurement techniques are now well established and ready to be employed for industrial applications. The large part of recent investigations is devoted to the enhancement of the quality and resolution of these techniques (improvements of image analysis methods) and to the extraction of useful information from the large amount of data provided (improvement in data extraction methods) (papers in PIV 95 and PIV 97). However, a fundamental question, which is also common to other optical measurements techniques such as the LDA (Laser Doppler Anemometry), is usually not considered in detail:

— to what extent the measurements obtained from the images of tracer particles reproduce the actual flow field ?

Usually, to follow velocity fluctuations, particles are required to be small enough and to have almost the same density of the flow: these requirements should be related to the small and large scales of the flow field. The previous question is especially important for investigations on the small scale structure of a turbulent flow, i.e. the field of velocity differences and related quantities. The problem is not so crucial for LDA measurements due to the fact that the tracer particles are sufficiently small (less than 5 μm) to capture almost all the vortical structures. On the other hand, in PIV and PTV, 10 times larger particles are used and the previous problem should be considered.

In this paper, velocity measurements are taken in the far field of a round jet in water using PTV to point out the behaviour of three different tracer particles which have densities lower, almost equal and larger than the fluid: air bubbles, pollen particles and sand grains. The interest is focused on the effect of a different particle density, rather than on the effect of different particle size, because the size range in PIV and PTV applications is quite limited to the specific fluid: 1-10 μm for measurements in air and 10-100 μm for measurements in water. Apart from the evaluation of velocity moments, attention is devoted to the computation of velocity differences and in

particular to its moments for increasing separation distances (that is for different scales of the flow field).

2. Theoretical Background

The motion of solid particles is usually investigated in the low concentration regime, i.e. in the case in which particles interact with the flow field but not between them (one-way coupling, Elgobashi, 1994). This hypothesis is valid for particle concentration C much smaller than unity. Therefore, it is reasonably fulfilled in PTV ($C \approx 10^{-3}$) and even in PIV ($C \approx 10^{-2}$). In this regime, assuming isotropic and homogeneous turbulence, a small particle Reynolds number (that is a small difference between particle and flow velocity), spherical particles and neglecting the viscous contributions (which means a particle diameter much lower than the flow smallest scale), it is possible to obtain the Basset-Boussinesq-Oseen (hereafter BBO) equation (Corrsin and Lumley, 1956; Maxey and Riley, 1983; Merzkirch, 1987):

$$\left(\frac{d\underline{u}_p}{dt}\right) + a\underline{u}_p = a\underline{u}_f + b\frac{d\underline{u}_f}{dt} + c\int_{t_o}^{t} \frac{1}{(t-\tau)^{1/2}} \frac{d}{d\tau}\left(\underline{u}_f - \underline{u}_p\right) d\tau \qquad (1)$$

where u is the velocity, t the time (t_0 is the initial time) and the indexes p and f refer to the particle and the fluid respectively. The quantities a, b and c are given by:

$$a = \frac{36\mu}{\left(2\rho_p + \rho_f\right)d^2},\ b = \frac{3\rho_f}{2\rho_p + \rho_f},\ c = \frac{18}{\left(2\rho_p + \rho_f\right)d}\sqrt{\frac{\rho_f \mu}{\pi}}$$

where ρ is the density, μ the viscosity coefficient and d is the particle diameter. For the vertical velocity component (the one along the direction of the gravity force) there is an additional term $a'g$ (where $a' \approx (\rho_p - \rho_f)/\rho_p$ and g is the gravity acceleration). This term gives contribution only to the mean vertical velocity and not to fluctuations.

The BBO equation is an ordinary differential equation which can be solved to determine the velocity of a particle u_p for given values of a, b and c (that is for given flow and particles) once that the velocity flow field u_f is specified. Previous numerical computations revealed that the particles smooth flow fluctuations at high frequencies (Elgobashi and Truesdell, 1992). However, due to the number of assumptions made to derive Eq (1), it would be necessary to have some experimental result to compare with. In Section 4 of this paper, the BBO equation is solved for the particles used in this work and the results are compared to those obtained by the experiments.

3. Experimental Set-up and Data Analysis

The velocity measurements are performed on the far field of a round water jet at $x/D \approx 40$ (x is the axial direction and $D = 20$ mm is the jet diameter). At this distance from the outlet, isotropy in the inertial range is obtained: this has been verified by preliminary measurements in which the longitudinal and transverse velocity differences have been evaluated and compared (Romano et al., 1999). The experimental set-up is shown in Fig. 1. The contraction ratio is equal to 50 (in area) and it is designed to suppress the growth of Görtler vortices. The Reynolds number for the present tests is $Re = U_o D/\upsilon \approx 4.4' 10^4$ ($U_o = 2.5$ m/s is the axial mean velocity at the outlet) and the Taylor microscale Reynolds number is $Re_\lambda = u'\lambda/\upsilon \approx 500$ ($u' = 0.13$ m/s is the local rms of the axial velocity and $\lambda = 4$ mm is the Taylor microscale).

In order to have non-dimensional results, the Kolmogorov small scales are used: they are computed independently from the present measurements using the relation for the energy dissipation (ε) derived by Antonia et al. (1980) in a round jet at the same distance from the outlet and same Reynolds number using Hot Wire Anemometry:

$$\frac{\varepsilon D}{U_0^3} = C_1\left(\frac{x}{D}\right)^{-4}$$

where the constant C_1 is equal to 48. Therefore, the Kolmogorov scales for length and velocity are $\eta = (\upsilon^3/\varepsilon)^{1/4} \approx$

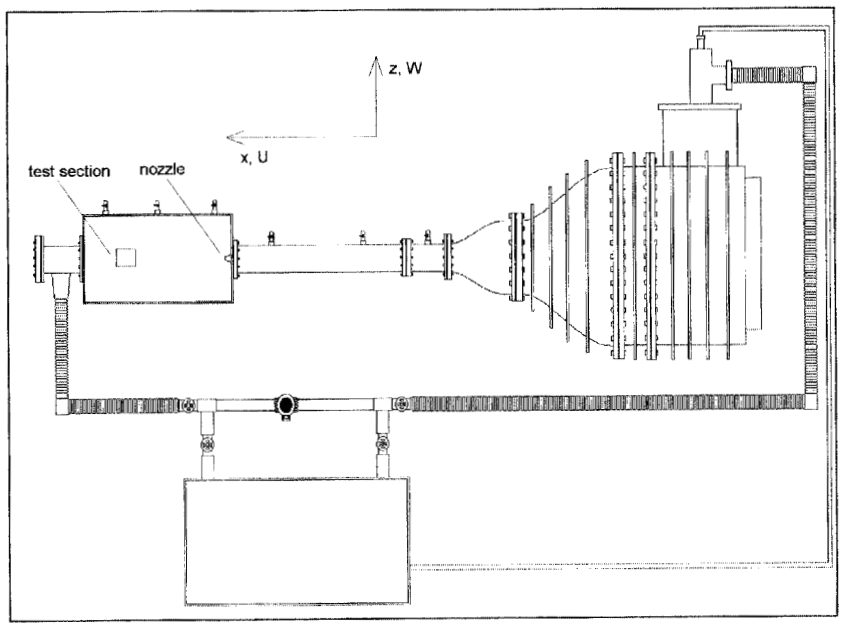

Fig. 1. Experimental set-up and reference frame.

0.1 mm and $v_K = (\upsilon\varepsilon)^{1/4} \approx 11$ mm/s.

The jet flows into a tank (height $\approx 30D$, width $\approx 30D$, length $\approx 60D$) and the light sheet for PTV measurements is located approximately at the middle of this tank. All the convergers, pipe and tank are made by transparent perpex to allow direct optical access: video cameras can be placed anyway around the tank. Previous PTV and LDA measurements confirm that the flow field is unaffected by external forcing frequencies (from the pump) and that it is axisymmetric without swirl (Romano, 1998).

Measurements by LDA (seeding particles size less than 3 μm) are used for comparison with PTV data (Taylor's hypothesis is applied to convert the temporal data to space): at this Reynolds number the IR determined from LDA is not expected to be affected by noise (Antonia et al., 1997).

The tracer particles are injected in the flow upstream of the converger (at 0.6 m, equal to $30D$). Preliminarily, the tank, where the test section is located, is seeded with tracer particles in order to obtain velocity measurements from both the jet and the ambient flows. The different tracer properties are given in Table 1 (the size of the sand grains is almost twice the others and the role of this effect will be discussed in the next section). The particle size was measured in-situ by a Phase Doppler Anemometer (PDA) which also gives the rms of the almost Gaussian size distribution (equal to about 20% of the mean). No special care was given to achieve a rather thin particle distribution because usually in PIV and PTV applications sizes are widely distributed. The particle time scale represents the time interval for a particle to reach about 60% of the velocity of the fluid. This means that the inverse of such a time is a cut-off frequency for fluctuations sensed by the particle. However, this parameter is sensitive only to the Stokes force (terms containing a in the BBO equation). For τ_p less than unity, Elgobashi (1994) predicted an increase of energy dissipation in the flow due to additional friction forces on the particles. The Stokes velocity is the characteristic rising (positive values) or settling (negative values) velocity of a particle under the Stokes force.

The test section is illuminated by an Ar-Ion beam which is reflected by a polygonal rotating mirror. Its angular velocity is selected so that only one image of each tracer particle per frame is detected (the time interval

Table 1. Physical properties of tracers: The particle time scale (t_p) is equal to $\rho_p d^2/18\upsilon\rho_f$ and the Stokes velocity (w_s) is equal to $-a'g\tau_p$.

Seeding	Density (gr/cm^3)	Size(μm)	τ_p (s)	w_s (mm/s)
Air	$1.2\ 10^{-3}$	40 ± 20	$1.33\ 10^{-5}$	1.06
Pollen	1.01	50 ± 20	$1.74\ 10^{-2}$	—0.02
Sand	2.01	100 ± 40	0.29	—5.51

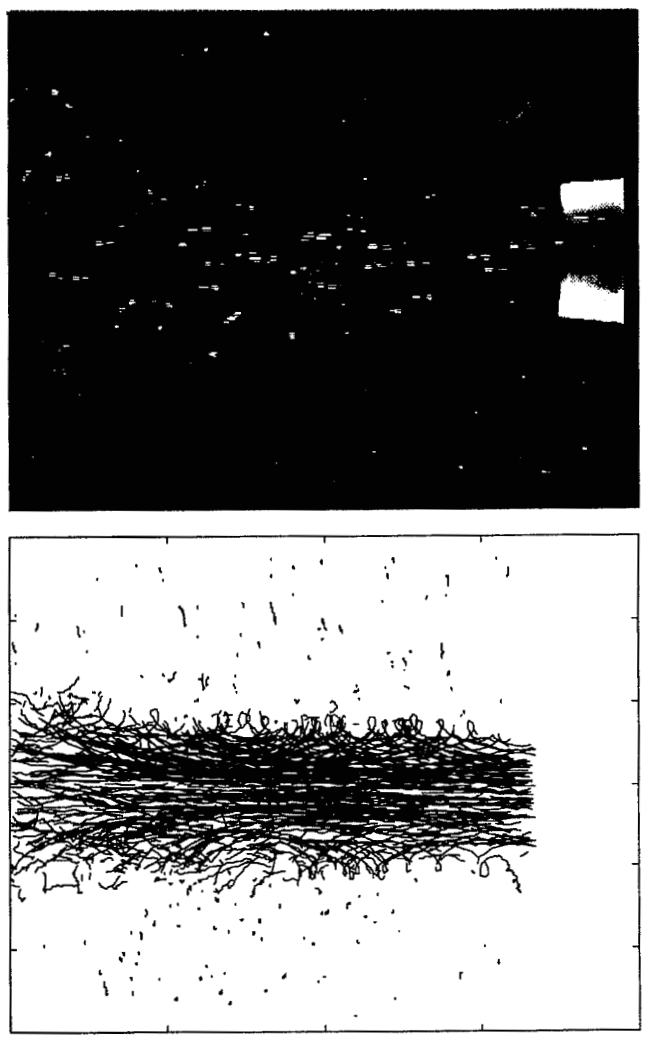

Fig. 2. Example of single frame acquisition (at the top) and of image analysis to determine particle trajectories (at the bottom).

between the beam pulses is 1 ms). The thickness of the light sheet is about 1 mm (0.05D) and the test section size

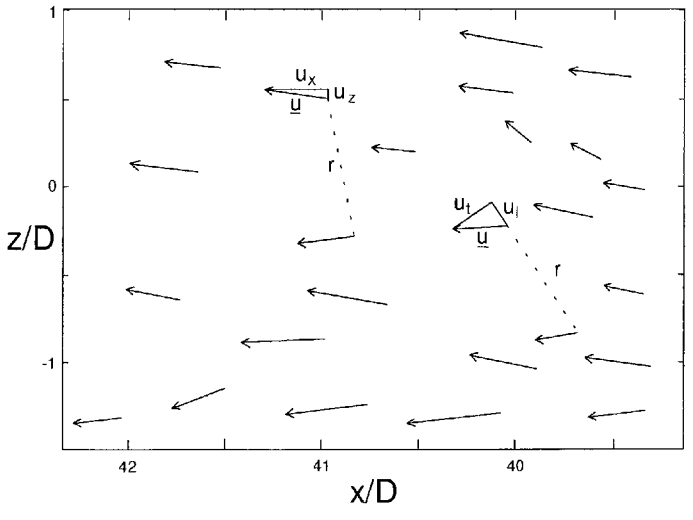

Fig. 3. An example of validated velocity vectors in the test section. Velocity components for computation of differences.

is 5.2 cm×4.6 cm.

The PTV images are acquired by a high-speed video camera (resolution equal to 480*420 pixel at a frame rate equal to 250 Hz) and recorded on a video-recorder for post-processing. In Fig. 2 an example of image acquisition and processing is given. The velocity components on the test section are evaluated using a frame by frame tracking of the particle images using two parameters: the maximum expected velocity and acceleration. As a result, positions and velocities of all particles belonging to the validated trajectories on each frame are recorded. The minimum detected displacement is in theory 0.1 mm (that is almost equal to the Kolmogorov scale) and the error on the velocity is less than 5%. However, due to the particle image size, the minimum displacement is about 0.4 mm (4η). In Fig. 3 an example of vectors is given: on the average about 30 trajectories are validated for each frame. Further details on the PTV procedure are given in Miozzi et al. (1998).

Velocity moments are computed from PTV images with the information being averaged over the whole range of flow scales. Even data from correlations and spectra allow only a few details on the flow scales to be derived (i.e. the slope in the inertial range). Therefore, from such moments it is difficult to evaluate the quality of the results from different tracer particles in respect to the flow behaviour. The quantities which can emphasise these aspects are the velocity structure functions (i.e. the moments of order n of the velocity difference between two points in space, which are also Galilean invariants) (Frisch, 1995):

$$\overline{\delta u_l^n(r)} = \overline{\left[u_l(x+r) - u_l(x)\right]^n}$$

$$\overline{\delta u_t^n(r)} = \overline{\left[u_t(x+r) - u_t(x)\right]^n}$$

where the overbar denotes average in time, r is the separation distance, u_l is the fluctuating velocity component along this direction (longitudinal structure functions) and u_t is the fluctuating velocity component in the orthogonal direction (transverse structure functions) (Fig. 3). Theoretical concerns lead to the following predictions (Frisch, 1995):

$$\overline{\delta u_l^{*3}} \approx 4r^*/5 \qquad \text{(for } 1 << r^* << L/\eta, \text{ inertial range)}$$

$$\overline{\delta u_{l,t}^{*n}} \approx r^{*n} \qquad \text{(for } r^* \approx 1, \text{ dissipative range).}$$

where L is the integral scale in length ($\approx$ 30 mm for the present measurements) and the asterisk denotes normalisation using Kolmogorov length and velocity. The first one of these predictions is used to evaluate the extension of the inertial range. Without considering intermittency corrections, the first of the previous predictions was extended to order $n \neq 3$ (Frisch, 1995):

$$\overline{\delta u_l^{*n}} \approx r^{*n/3} \qquad \text{(for } 1 << r^* << L/\eta, \text{ inertial range).}$$

(intermittency is accounted by considering non-linear exponents).

About 50000 images are collected to compute the previous statistics: the average number of data for each separation is about 10000. Although rather high, this number is not sufficient to compute high-order structure functions and results are given for second- and third-order only.

4. Predictions of Particle Behaviour

The integration of the BBO equation allows to obtain a prediction on the behaviour of the particles. The solution is obtained for a given sinusoidal flow velocity to which the particle responds with a still sinusoidal velocity but with different amplitude β and phase ϕ.

From preliminary solutions it was found that the effects of the terms a, b and c on the result are equally important especially for what concerns the phase: for example neglecting term c (Basset force) for the air bubbles leads to differences of the order of 20% in the amplitude and of 0.2 rad in phase. The situation is not so critical for what concerns the sand particles for which differences are within a few percents. Computations of the three variables a, b and c are given in Table 2 for the air and sand particles which are lighter and heavier than the fluid. The comparison between the results of the three tested approximations reveals differences (even for the sand particles) which cannot be discharged a priori. Therefore, to have reasonable predictions, none of the three terms

Table 2. Evaluation of the variables *a*, *b* and *c* for the sand and air particles using different approximations: the approximation 1 (App. I) corresponds to neglecting term *c* (Basset force), the approximation 2 (App. II) to a density of the particle much higher than that of the fluid and the approximation 3 (App. III) to neglecting term *b* (fluid velocity fluctuations).

sand	*a*	*b*	*c*
All terms	717	0.598	20.2
App. Ⅰ	717	0.598	0
App. Ⅱ	896	0.746	0
App. Ⅲ	896	0	0
air	***a***	***b***	***c***
All terms	$2.2\ 10^4$	2.99	253
App. Ⅰ	$2.2\ 10^4$	2.99	0
App. Ⅱ	$9.4\ 10^6$	833	0
App. Ⅲ	$9.4\ 10^6$	0	0

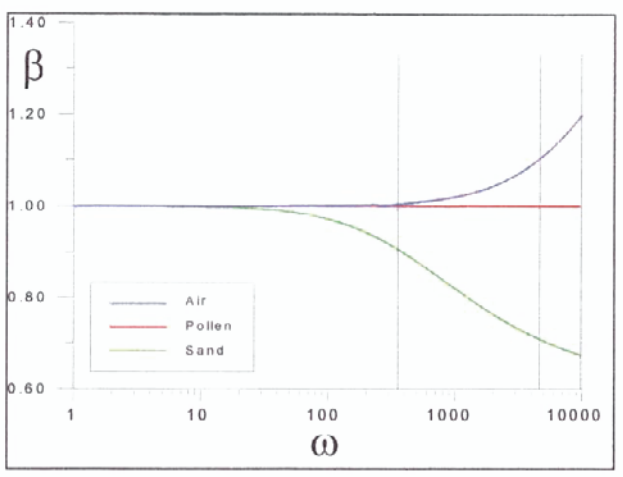

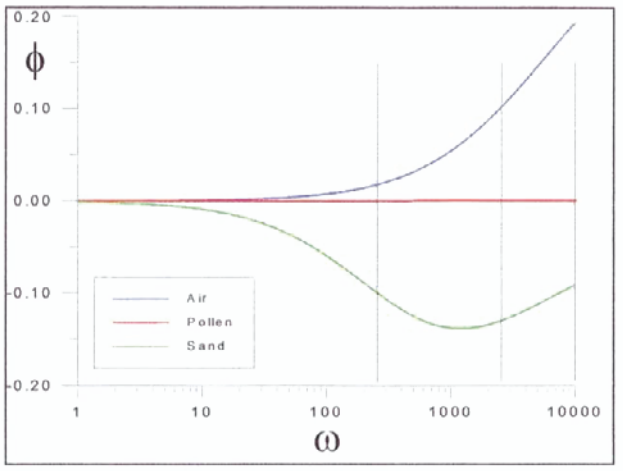

Fig. 4. Amplitude and phase of the particle velocity computed from the BBO equation. Cut-off pulsations are shown by vertical dotted lines.

containing the quantities *a*, *b* and *c* can be neglected and the BBO equation is solved in its general form. In Fig. 4 the amplitude and phase of the particle velocities for the tracers used in the present experiments (given in Table 1) are shown.

From the plot of the amplitude, the cut-off frequencies (defined as the frequency where the amplitude differs more than ±10% from unity) for the three seedings are computed: $f_{air} = \omega/2\pi \approx 800$ Hz, $f_{pollen} > 2$ kHz and $f_{sand} \approx 50$ Hz. These values are more than one order of magnitude different from those that can be derived from Table 1 using the particle time scale τ_p. This is especially true for the air bubbles which emphasise enhancements

rather than reductions of the amplitude. This is due to the fact that the particle time scale accounts only for one of the terms in the BBO equation. The behaviour of the phase (second part of Fig. 4) shows that the cut-off frequencies are slightly smaller than those from the amplitude (changes in the flow velocity are sensed by the particles with a delay in time even when fluid and particles have similar amplitudes). The previous frequencies are equivalent to the non-dimensional spatial separations r^* through the relation $r^* = U_l/f\eta$ (where U_l is the local mean velocity $\approx$ 35 cm/s): $r^* \approx 5$ (air), $r^* < 1$ (pollen) and $r^* \approx 70$ (sand). It is important to notice that if the computations are repeated using sand grains having a mean size equal to 50 μm (similar to that used for pollen particles and air bubbles), the cut-off frequency is about 200 Hz and the spatial separation is equal to 20 (it should also be considered that the particle size distribution is rather wide and covers the range from 30 μm to 70 μm around the mean size). These values are not so different from those obtained with the larger sand grains, thus confirming the main role of the relative density in the size range used in PIV and PTV.

5. Results

As expected, very small differences are observed between the results from velocity moments obtained using the different tracer particles. Results are given in Table 3 together with results from LDA measurements at the same position. The results are very similar except for the mean vertical velocity which is positive for air bubbles, negative for the sand and almost zero for the pollen, as from LDA measurements: this is in agreement with predictions from the values of the Stokes velocity (given in Table 1). Differences are observed also in the skewness of both velocity components especially for air bubbles: this indicates some preference towards negative longitudinal and positive vertical fluctuations (in comparison to the mean values). To this end, although larger and heavier, the sand particles give values in better agreement with LDA. However, the best agreement with LDA is obtained using the pollen particles. This preliminary conclusion is supported by the analysis of the probability density distributions of velocity fluctuations given in Fig. 5 (on a semi-log plot). Both distributions obtained with the sand grains and the air bubbles are quite different from that obtained with the pollen particles especially for what concerns the very infrequent events characterised by velocities far from the mean value. These events are captured due to the huge amount of images acquired in the present measurements. Therefore, even if the statistics obtained with the different tracers are similar, the detailed flow descriptions seem to be different as will be shown in the following. The differences are more pronounced for the velocity component orthogonal to the mean flow in comparison to the streamwise component.

The results from correlation and spectral functions (not shown) are also very similar. The major differences between the results are observed when velocity differences are considered: the turbulent kinetic energy dissipation (assuming isotropy) is $\varepsilon \approx 120$ cm^2/s^3 for measurements using air bubbles or sand, while it is $\varepsilon \approx 61$ cm^2/s^3 for pollen. Antonia et al. (1980) measurements in similar conditions gave $\varepsilon \approx 70$ cm^2/s^3, so that an overestimation of the energy dissipation is obtained when using air bubbles or sand as predicted by Elgobashi (1994).

A similar difference is observed when structure functions are evaluated (structure functions represent moments of velocity differences). In Fig. 6, the non-dimensional second-order ($n = 2$) longitudinal and transverse structure functions are reported for the different tracers. While all curves seem to collapse for $r^* > 60$ (towards the large scales), differences are observed for $r^* < 40$ (towards the lower part of the inertial range and the dissipative

Table 3. First four moments of longitudinal and vertical velocity components. Comparison with results from LDA at the same position.

	U(mm/s)	σ_u/U	Skew	Flat
Air	355	0.31	−0.288	2.70
Pollen	298	0.32	−0.168	2.82
Sand	355	0.31	−0.256	2.81
LDA	304	0.31	−0.145	2.71

	W(mm/s)	σ_w/U	Skew	Flat
Air	3.22	0.25	−0.156	2.96
Pollen	−1.88	0.25	0.011	2.89
Sand	−6.86	0.26	0.012	3.08
LDA	−2.32	0.24	0.006	2.88

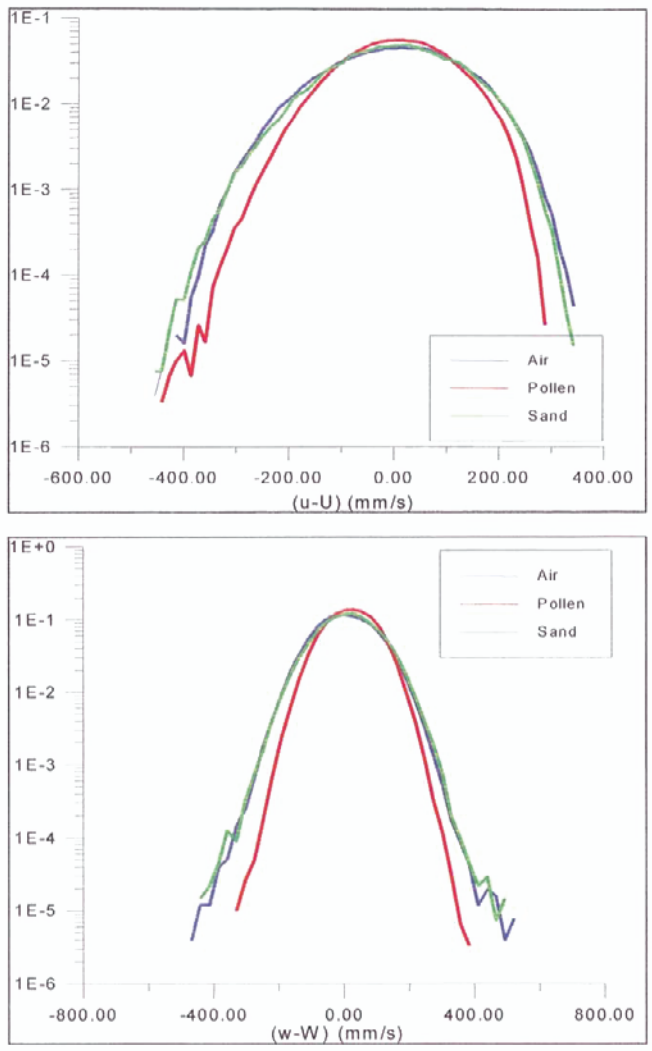

Fig. 5. Probability density distributions for the three tracers in the measurement region: longitudinal velocity component (at the top) and vertical velocity component (at the bottom).

range). For $r^* < 10$ and $r^* > 500$ a poor sample number leads to data oscillations: these boundaries are related to the minimum and maximum detectable separations. Both for longitudinal and transverse structure functions, the results from pollen particles are those which better compared to LDA. For $r^* > 10$ differences are observed between the longitudinal and the transverse structure functions: in the former, the results from air and sand depart from those of pollen, whereas in the latter, the results from sand approach better those by pollen. Considering that structure functions involve only fluctuating velocities, these findings are in agreement with results obtained from moments (Table 3) and probability density distributions (Fig. 5) (which are averaged over the whole range of scales) and from energy dissipation (which mainly depends on the small scales). From this kind of plot, it is difficult to precisely determine the extension of the inertial range.

Based on the theoretical predictions given in Section 3, the third-order longitudinal structure function must scale as the separation r^* (and this result is independent of intermittency effects). In Fig. 7, the third-order longitudinal structure function divided by r^* is plotted for the different acquisitions. To avoid strong oscillations due to the poor sample number, the absolute value of the third-order structure function is computed. Antonia et al. (1998) have shown that, when using third-order absolute rather than non-absolute structure functions, although the values obtained are different, the extension of the inertial range is unaffected. In Fig. 7 it can be observed that not only the shape of the curves but also the extensions of the inertial ranges are different. The results from LDA indicate that this range is from $r^* \approx 20$ to $r^* \approx 115$, in agreement with results obtained using Hot Wire in similar conditions which indicate $35 \leq r^* \leq 130$ (Romano et al., 1999). The following inertial ranges are derived from the different particles:

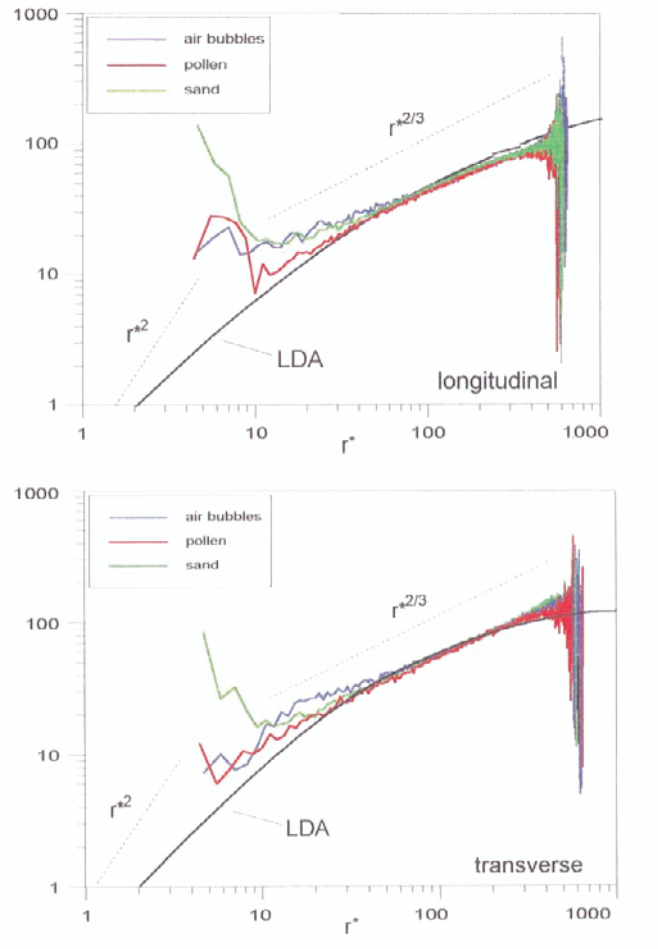

Fig. 6. Second-order longitudinal and transverse structure functions evaluated from PTV measurements using the different tracer particles. Results from LDA and theoretical slopes in dissipative and inertial ranges are also shown.

- air bubbles $30 \leq r^* \leq 55$
- pollen particles $15 \leq r^* \leq 110$
- sand grains $45 \leq r^* \leq 110$

As for the other quantities, the pollen particles give the best representation of both the lower and higher boundary of this range. The lower boundary resulting for the sand grains is in good agreement with findings from the computation of the BBO equation given in Section 4. The results from sand particles also reproduce quite well the higher part of the inertial range. On the other hand, the air bubbles are not able to detect velocity differences for $r^* < 30$, while the prediction from the solution of the BBO equation suggests no deformation for $r^* > 5$. This discrepancy is probably due to the strong assumptions made to derive the BBO equation (nevertheless the result is quite good for the order of magnitude of the frequencies involved). More surprisingly, the result from the air-bubbles indicates deviations also for the higher boundary of the inertial range and even for all the range of the large scales. This means that these particles are not able to capture both small, intermediate and large scale velocity fluctuations.

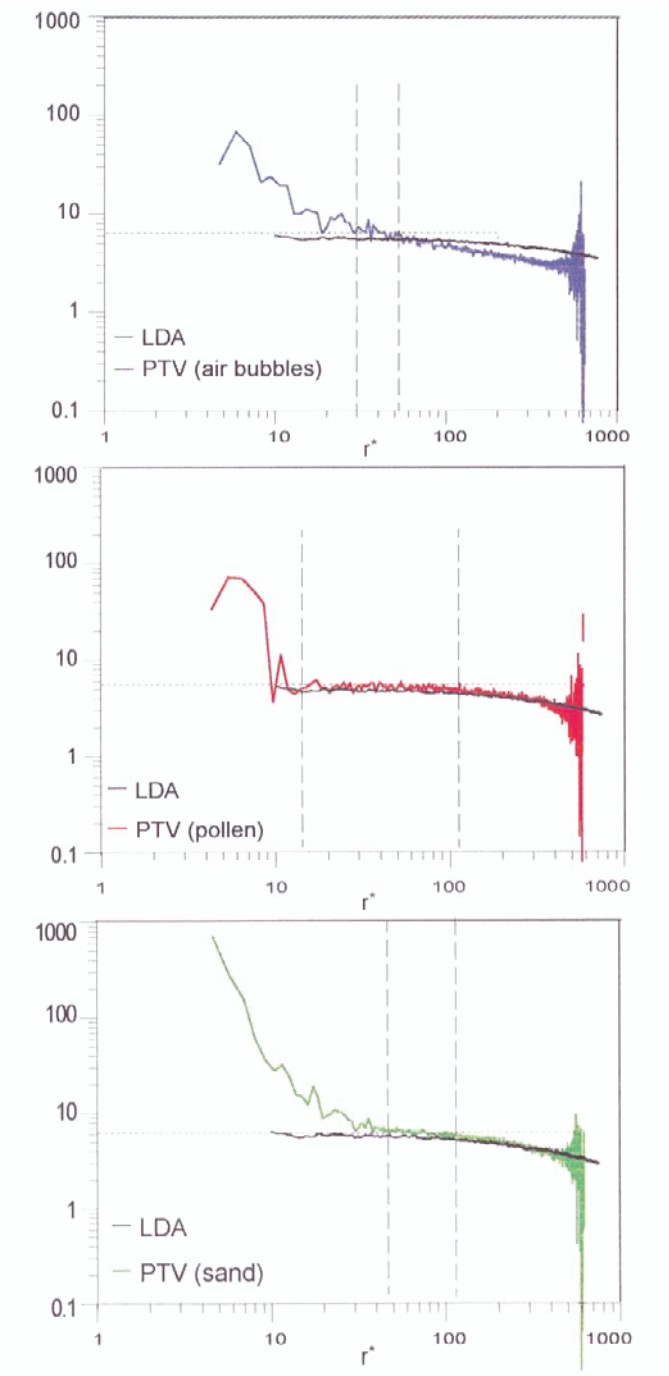

Fig. 7. Third-order longitudinal and transverse structure functions divided by r^*, evaluated from PTV measurements using the different tracer particles. The vertical dotted lines bound the different inertial ranges. Results from LDA are also shown.

6. Conclusions

In this paper the PTV technique is used to point out the effect on the velocity field of using different tracer particles. Although the question is of fundamental importance in defining the reliability of the data, it is usually inadequately considered. The measurements are performed on a round water jet and the quantities which are measured are the moments of the velocity differences representing the flow behaviour on the whole range of scales (structure functions). PTV enables to determine this behaviour in space rather than in time as by conventional single-point methods as LDA (which need the use of Taylor's hypothesis to transform the time behaviour in space).

The tracer particle density is found to strongly influence the results (while the particle size is not changed due to the fact that it is basically determined by the measurement technique): particles with density higher than that of the fluid behave much better than those with lower density. While the former loose only the small-scale (high frequency) behaviour, the latter are not able to reproduce satisfactorily the whole range of scales. However, being mean values, standard deviation and other one-point moments averaged over the flow scales, they are still very similar also when using different tracers. This compensation could hide the deformation of the flow field when making measurements based only on one-point moments. Velocity probability density distributions computed using a large number of data can clarify the reliability of the measurements.

Predictions are possible using a simplified equation (the Basset-Boussinesq-Oseen equation) which describes the behaviour of a single particle in the fluid. These predictions are in good agreement with findings from the present PTV measurements.

Acknowledgments

The authors acknowledge the support of MURST.

References

Antonia, R. A., Satyaprakash, B. R. and Hussain, A. K. M. F., Measurement of dissipation rate and some other characteristics of a turbulent plane and circular jets, Phys Fluids, 23 (1980), 695-699.

Antonia, R. A., Zhou, T. and Romano, G. P., Second- and third-order longitudinal structure function in a fully developed turbulent channel flow, Phys Fluids, 9-11 (1997), 3465-3471.

Antonia, R. A., Zhou, T. and Zhu, Y., Three-component vorticity measurements in a turbulent grid flow, J Fluid Mech, 374 (1998), 29-57.

Corrsin, S. and Lumley, J., Appl Sci Research, 6A (1956) , 114-123.

Elgobashi, S. and Truesdell, G.C., Direct simulation of particle dispersion in a decaying isotropic turbulence, J Fluid Mech, 242 (1992), 655-700.

Elgobashi, S., On predicting particle-laden turbolent flows, App Sci Research, 52 (1994), 309-329.

Frisch, U., Turbulence: the legacy of A.N. Kolmogorov, (1995), Cambridge University Press.

Maxey, M. and Riley, R., Equation of motion for a small rigid sphere in a nonuniform flow, Phys Fluids, 26 (1983), 883-889.

Merzkirch, W., Flow Visualizations, (1987), Academic Press.

Miozzi, M., Querzoli, G. and Romano, G. P., The investigation of an unstable convective flow using optical methods, Phys Fluids, 10-11 (1998), 2995-3008.

PIV 95, Proceedings of the First International Workshop on PIV, (1995), Fukui (Japan).

PIV 97, Proceedings of the Second International Workshop on PIV, (1997), Fukui (Japan).

Romano, G. P., Investigation on particle trajectories and lagrangian statistics at the outlet of a circular jet, Exp Thermal Fluid Science, 17 (1998), 116-123.

Romano, G. P., Turano, E. and Antonia, R. A., The measurement of longitudinal and transverse structure functions in a turbulent round jet, Proceedings of the First International Symposium on Turbulence and Shear Flow Phenomena, (1999), Santa Barbara (USA).

Author Profile

Giovanni P. Romano: He received his degree in Physics in 1984 from University "La Sapienza" in Roma. He worked at the Italian Towing Tank Institute (INSEAN) on Naval Hydrodynamics from 1985 to 1989. Since 1989 is at the Department of Mechanics and Aeronautics of the University "La Sapienza" in Roma as Research Scientist (teaching Numerical Fluid Mechanics) and from 1998 as Professor of Experimental Aerodynamics. He is involved in research project for the investigation of large and small-scale structures in turbulent flows as jets, boundary layers, channel flows and wakes using optical techniques as LDA, LIF, PTV and PIV. He published more than 20 papers in International Journals.

Stefano Zincone: He got his degree in Aeronautical Engineering in December 1998 and at present collaborates with the Department of Mechanics and Aeronautics.